J Solid State Electrochem (2011) 15:485–491
DOI 10.1007/s10008-010-1108-7

ORIGINAL PAPER

A hierarchical porous MnO_2-based electrode for electrochemical capacitor

Leigang Xue · Hao Hao · Zhen Wei · Tao Huang · Aishui Yu

Received: 30 March 2010 / Revised: 10 May 2010 / Accepted: 15 May 2010 / Published online: 26 May 2010

Abstract A hierarchical porous MnO_2-based electrode was prepared and its electrochemical performance for electrochemical capacitors was investigated. In this work, porous MnO_2 film with pore size of 2–3 nm in diameter was deposited on a three-dimensional porous current collector by cathodic electrodeposition associated with subsequent controlled heat treatment at 200°C for 2 h. Transmission electron microscopy and X-ray photoelectron spectroscopy showed that the heat treatment has a great effect on the formation of the porous structure of MnO_2 layer, and the disordered porous structure was caused by dehydration during the heat treatment. Cyclic voltammetry and galvanostatic charge–discharge tests showed that both energy and power densities are enhanced due to the unique hierarchical porous structure. The electrode delivers a high specific capacitance of 385 F g^{-1} at a high current density of 5 A g^{-1} within a potential window of −0.05 ~ 0.85 V, and also exhibits excellent rate capability and electrochemical stability.

Keywords Manganese dioxide · Three-dimensional porous current collector · Utilization efficiency · Electrochemical capacitor

Introduction

Electrochemical capacitors (ECs), as a kind of fast and high-power charge storage device, have attracted great interest due to their potential in complementing or replacing batteries in future energy storage systems [1–4]. ECs offer power densities 1,000-fold greater than that of batteries; however, their energy densities are typically about 10- to 100-fold smaller [5]. Therefore, most researches on ECs are focused to improve their energy densities [6–8]. Manganese dioxide is a promising active material in ECs because of its natural abundance, environmental compatibility, low cost, and high theoretical specific capacitance (SC) of 1,370 F g^{-1} expected for a redox process involving one electron per manganese atom [9–11]. However, its practical SC is still low compared with the high-cost RuO_2 which shows much higher SC of more than 600 F g^{-1}. It is believed that the low energy density of MnO_2 is caused by its charge storage mechanism, which is based on ion adsorption or redox reactions on the surface layer [11–13]. In a typical charge–discharge process of pseudocapacitors, only the first few nanometers from the surface can be utilized while no reactions occur in the bulk of active material, resulting in low utilization and limited energy densities [14–16]. Therefore, improving utilization efficiency of active materials is the key to enhance energy densities of pseudocapacitors. Consequently, porous materials, which can facilitate electrolyte ions to react with active materials more efficiently, have attracted great interest [17–22].

Pang et al. reported sol–gel-derived MnO_2 thin film electrode exhibits a high SC of 698 F g^{-1} at a loading of 1.05 μg cm^{-2} [12]. At such a low thickness, almost complete utilization of active material occurs. However, thin layers of MnO_2 are uneconomical for practical applications, and hence, it would be beneficial if high values of SC can be obtained at higher loading levels [16]. From this point of view, if three-dimensional (3D) porous current collector is employed, the loading level of active material can be improved and the thickness still remains

L. Xue · H. Hao · Z. Wei · T. Huang · A. Yu (✉)
Department of Chemistry, Shanghai Key Laboratory of Molecular Catalysis and Innovative Materials, Institute of New Energy, Fudan University,
Shanghai 200438, China
e-mail: asyu@fudan.edu.cn

very thin because the 3D porous current collector has much bigger surface area compared to planar current collector, even though their nominal areas are the same. In addition, owing to the big contact area between the active materials and the 3D porous current collector, higher cohesion and lower contact impedance could also be achieved.

Based on the above analysis, we proposed a design strategy for preparation of an electrode for ECs. It can be illustrated as in Fig. 1, a 3D porous substrate is adopted as the current collector on which porous active materials are coated. This design combines the advantages of porous active materials and 3D porous current collector. For the as-designed hierarchical porous electrode, electrolyte ions can easily transport through and react with active materials and thus improve utilization efficiency of active material and enhance corresponding SC accordingly. In this work, a gold-coated Ni foam was used as the current collector on which porous MnO_2 was coated by cathodic electrodeposition with subsequent heat treatment. The electrochemical performance of the electrode was studied.

Experimental

Preparation of the MnO_2-based electrode

Electrodeposition was performed on a CHI660C electrochemical workstation (CH Instruments, Shanghai) using a four-electrode system. The working electrode is a gold-coated Ni foam (1×1 cm) and placed symmetrically between two Pt-coated Ti plates auxiliary electrodes (Pt/Ti, 1.5×1.5 cm). A saturated calomel electrode (SCE) was used as reference electrode. The MnO_2 films were electrodeposited in a $KMnO_4$ solution (0.1 M) potentiostatically at −0.1 V or galvanostatically at 10 mA cm^{-2} without stirring at ambient temperature. The as-deposited electrodes were washed with deionized water and then heated at 200°C and 400°C for 2 h in ambient atmosphere, respectively.

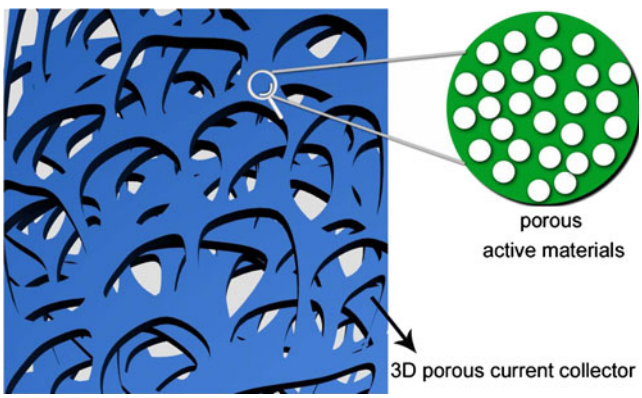

Fig. 1 Schematic representation of the designed electrode

Characterization and electrochemical measurements

The morphology of the gold-coated Ni foam was observed using a Philip XL30 scanning electron microscope (SEM). The cathodically electrodeposited MnO_2 films were scraped off from the current collector and ultrasonically dispersed in methanol for 5 min, a drop of this mixture was placed on a copper grid covered with a carbon coating and it was allowed to dry in air, and then imaged by transmission electron microscopy (TEM, JEOL JEM-2100 F) with an accelerating voltage of 200 kV. X-ray photoelectron spectroscopy (XPS) was recorded under ultrahigh vacuum ($<10^{-6}$ Pa) at a pass energy of 93.90 eV on a Perkin–Elmer PHI 5000C ESCA system equipped with a dual X-ray source by using Mg K_α(1,253.6 eV) anode and a hemispherical energy analyzer. All binding energies were calibrated with contaminant carbon (C1s=284.6 eV) as a reference. The electrochemical performances of electrodes were characterized by a CHI660C electrochemical workstation and a potentiostat/galvanostat (Wuhan Land Electronic Co., Ltd.) at constant temperature of 25°C. A conventional three-electrode system was used, in which a Pt/Ti electrode (1.5×1.5 cm) and the SCE were used as counter and reference electrodes. The electrolyte used was 1 M Na_2SO_4. All potentials in the present study are reported against the SCE.

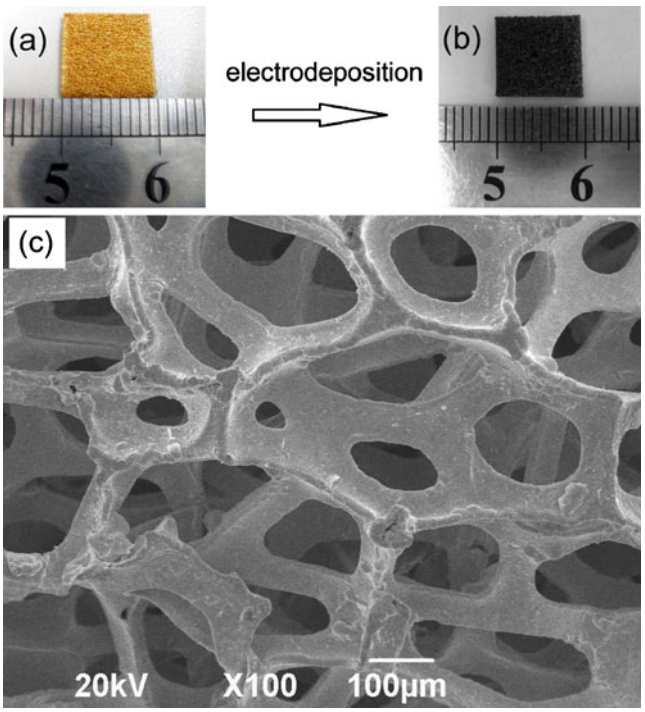

Fig. 2 Photographs of the gold-coated Ni foam before (**a**) and after (**b**) electrodeposition of MnO_2, and SEM image of the gold-coated Ni foam (**c**)

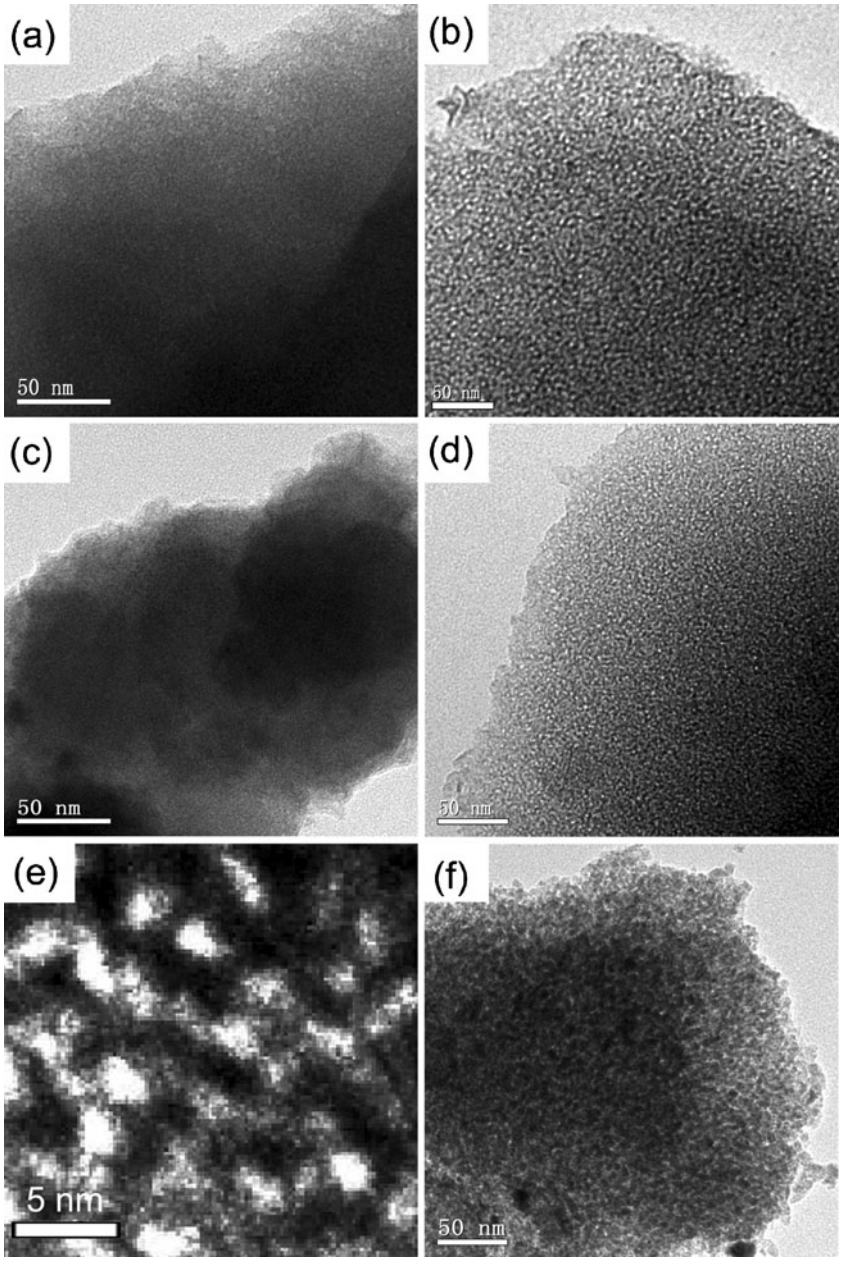

Fig. 3 TEM images of MnO_2 films electrodeposited at 10 mA cm^{-2} before heat treatment (**a**) and heated at 200°C for 2 h (**b**); electrodeposited at −0.1 V before heat treatment (**c**) and heated at 200°C for 2 h with different magnifications (**d**, **e**), electrodeposited at −0.1 V and heated at 400°C for 2 h (**f**)

$KMnO_4$ and Na_2SO_4 were purchased from Shanghai Chemical Reagent Co. LTD and used as received without further purification and all aqueous solutions were prepared using deionized water.

Results and discussion

Shown in Fig. 2a, c is a photograph and SEM image of the gold-coated Ni foam. It is a cellular structure composed of interconnected macropores with diameter of 50–200 μm. On the ligaments, which constitute the interconnected macropores, a black thin film of MnO_2 was coated by electrodeposition (Fig. 2b). Figure 3a is the TEM image of the MnO_2 film cathodically electrodeposited at constant current density of 10 mA cm^{-2}. It can be seen that the as-deposited film is a flat film; however, after calcination at 200°C for 2 h, disordered pores with diameters of 2 to 3 nm are randomly distributed on the heat-treated film (Fig. 3b). Potentiostatic technique was also employed to prepare the MnO_2 film. The TEM images of the MnO_2 films electrodeposited at −0.1 V before and after calcination are respectively shown in Fig. 3c–e. Just like the films prepared by galvanostatic technique, the disordered porous structure can only be formed after heat treatment. According to these results, it can be concluded that the heat treatment has a great effect on the formation of the porous structure. However, in further increasing heating temperature to

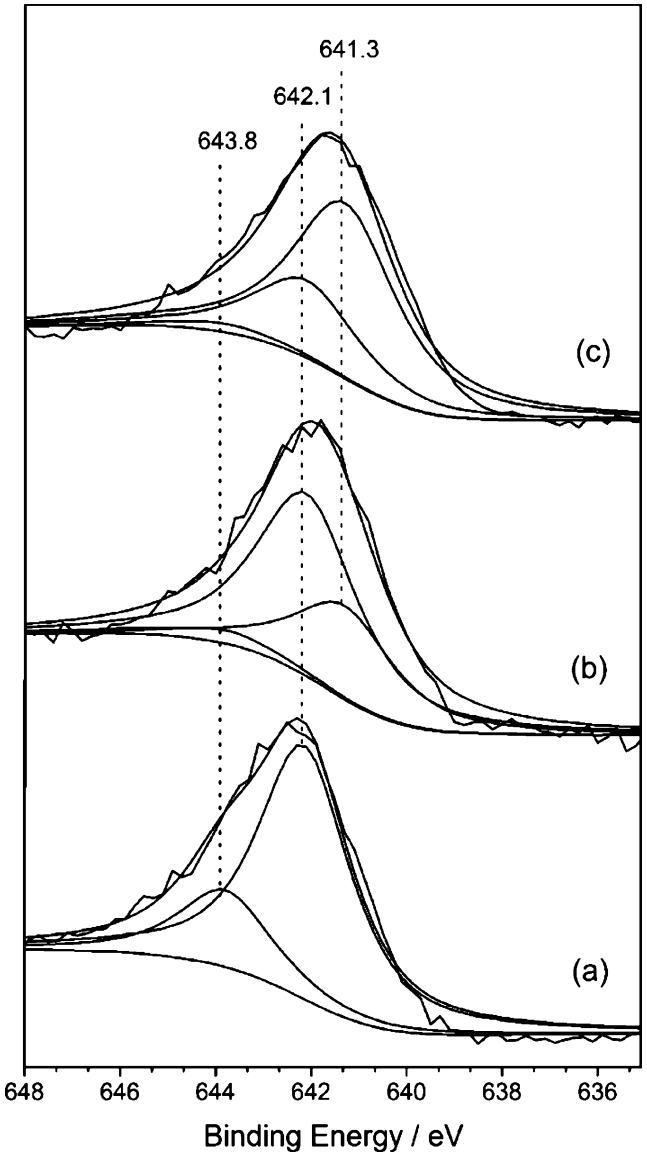

Fig. 4 $Mn_{2p3/2}$ XPS spectra of MnO_2 films cathodically electrodeposited at −0.1 V before heat treatment (**a**), heated at 200°C for 2 h (**b**), and heated at 400°C for 2 h (**c**). The *jagged lines* represent the spectral data while the *smooth lines* that overlay the spectral data represent the sum of the symmetric contributions (also shown) used to fit the respective spectra

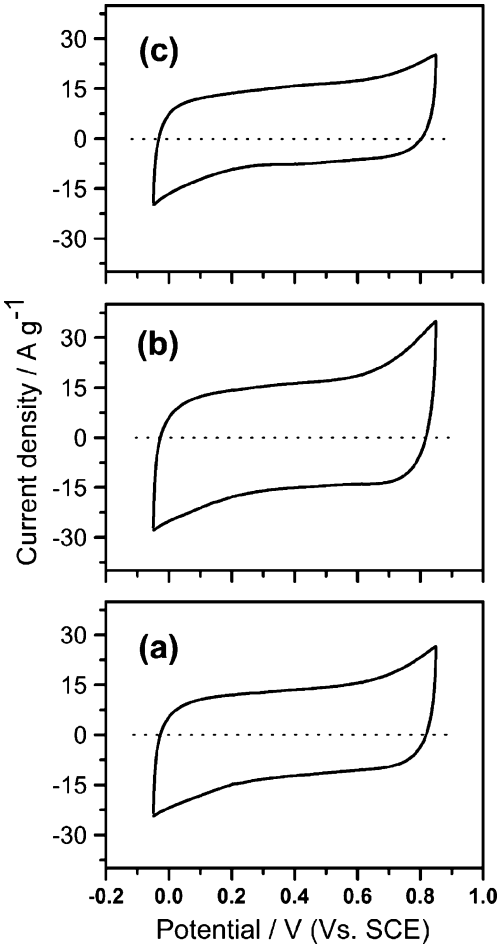

Fig. 5 CVs of the MnO_2-based electrodes before heat treatment (**a**), heated at 200°C for 2 h (**b**), and heated at 400°C for 2 h (**c**)

400°C, particles begin to aggregate and the amount of pores decreases (Fig. 3f).

Besides the formation of the disordered porous structure, the composition and oxidation states of the MnO_2 film may also change during the heat treatment [23–25] because transition metal atoms can exist in various oxidation states. $Mn_{2p3/2}$ XPS spectra were employed to analyze the oxidation states of MnO_2 films with various heating temperatures (Fig. 4). For all the samples, their XPS spectra are unsymmetrical and can be deconvoluted into three components at 643.8, 642.1, and 641.3 eV, corresponding to binding energies of Mn(IV)–OH, Mn(IV)–O, and Mn

Table 1 Proportions of components and average oxidation states for manganese oxide films cathodically electrodeposited at −0.1 V before heat treatment (**a**), heated at 200°C for 2 h (**b**), and heated at 400°C for 2 h (**c**)

	Mn(IV)–OH 643.8eV (%)	Mn(IV)–O 642.1eV (%)	Mn(III)–O 641.3eV (%)	Average oxidation state (AOS)
(a) Before heat treatment	23.3	76.7	0	4.0^+
(b) Heated at 200°C for 2 h	4.5	63.1	32.4	3.7^+
(c) Heated at 400°C for 2 h	3.3	29.6	67.1	3.3^+

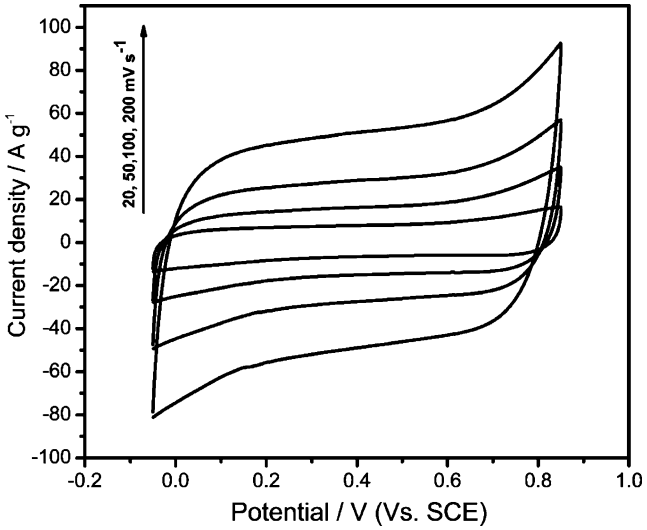

Fig. 6 CVs of the MnO_2-based electrode heated at 200°C for 2 h, where *arrow* indicates direction of increasing scan rates from 20, 50, 100, to 200 mV s^{-1}

(III)–O, respectively. Their molar percentages, which can be estimated from peak area of each component, were given in Table 1. For the as-deposited film, the majority of Mn (76.7%) is in the state of Mn(IV)–O with 23.3% of Mn (IV)–OH, all Mn exists in Mn(IV) oxidation state. After calcination at 200°C for 2 h, Mn(IV) is partially (32.4%) transformed to Mn(III), meanwhile, Mn(IV)–OH is almost disappeared. The average oxidation state (AOS) of manganese oxide is 3.7^+ and MnO_2 is still the main component. Further heat-treated at 400°C for 2 h, 67.1% of Mn(IV) transforms to Mn(III)–O, meaning Mn_2O_3 has become the main component, its AOS is 3.3^+.

As known from TEM and XPS analysis, the porous structure can be formed after calcination at 200°C for 2 h, and Mn(IV)–OH almost disappeared after this heat treatment. Therefore, we proposed that the formation of the porous structure is a result of dehydration during the heat treatment. It is important to note that in further raising the heating temperature to 400°C, Mn_2O_3 becomes the main component, and Mn_2O_3 particles tend to aggregate to form dense particles; as a result, the pore size becomes smaller and the porosity decreases, which is in conformity with the previous report [24].

The electrochemical properties of the MnO_2 electrodes prepared at 10 mA cm^{-2} and −0.1 V were tested and we found they have similar electrochemical performances, so, we introduced that prepared at −0.1 V here as an example. Figure 5 shows cyclic voltammograms (CVs) of the MnO_2-based electrode with different heating temperatures at a potential scan rate of 50 mV s^{-1}. The discharge capacitances which are directly proportional to the areas of discharge processes of CVs are different. The discharge capacitance of the electrode heated at 200°C for 2 h is much bigger than the other two. This result can be explained as follows: for the

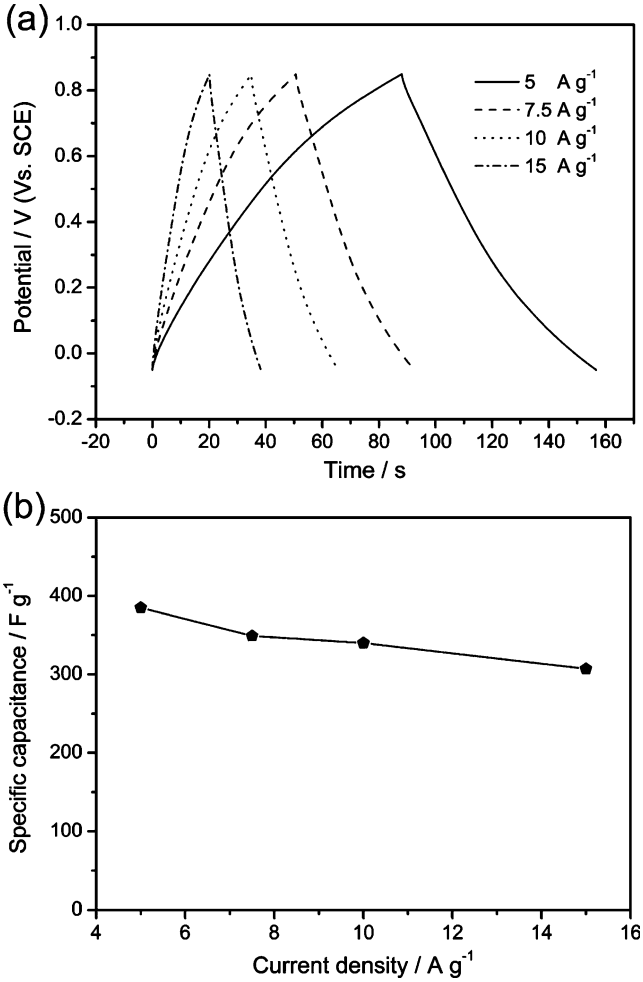

Fig. 7 Galvanostatic charge–discharge curves (**a**) and specific capacitances (**b**) at different current densities within a potential window of −0.05 to 0.85 V

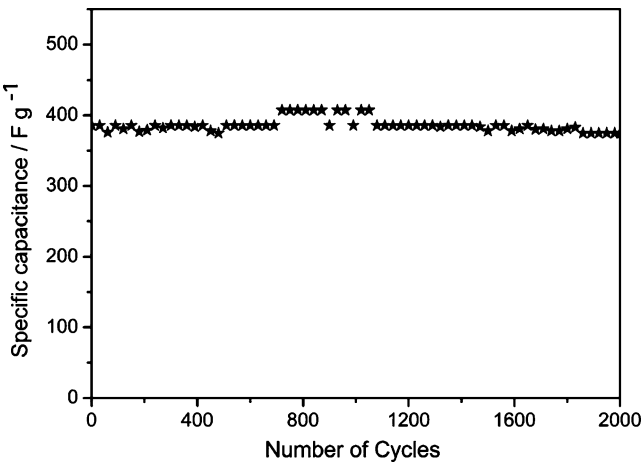

Fig. 8 Cycle life data at a charge–discharge current density of 5 A g^{-1} within a potential window of −0.05 to 0.85 V

untreated MnO_2 film, porous structure has not formed; for the manganese oxide electrode heated at 400°C for 2 h, Mn_2O_3 which has no capacitive behavior has become the main component; whereas the electrode after calcination at 200°C for 2 h is a MnO_2 electrode and the porous structure has formed. The results of CV test are in good agreement with TEM and XPS analysis.

The CVs at various potential scan rates from 20 to 200 mV s^{-1} for the MnO_2-based electrode heated at 200°C for 2 h is shown in Fig. 6. A potential window of −0.05 ~ 0.85 V was chosen to ensure the highest stability and reversibility of the redox process. No obvious distortion in the CVs is observed as the potential scan rate is increased; the curves are all rectangular in shape even at a high potential scan rate of 200 mV s^{-1}, indicating that the as-prepared hierarchical porous MnO_2-based electrode has a good rate capability [26].

Figure 7a gives the charge–discharge curves of the electrode at different current densities. The slight curvature of the charge–discharge curves indicates that the capacitance of MnO_2 mainly results from a pseudofaradaic reaction. According the previous reports [5, 14, 26], the redox charge storage mechanism of MnO_2 in neutral Na_2SO_4 aqueous electrolyte occurs via insertion–deinsertion of sodium ions

$$Mn^{IV}O_2 + Na^+ + e^- \rightleftarrows Mn^{III}OONa \quad (1)$$

or by surface adsorption via

$$\left(Mn^{IV}O_2\right)_{surface} + Na^+ + e^- \rightleftarrows \left(Mn^{III}O_2^-Na^+\right)_{surface} \quad (2)$$

Their specific capacitances can be calculated using the following formula [27]:

$$C_m = \frac{C}{m} = \frac{I \times t}{\Delta V \times m}$$

where C_m is the SC (F g^{-1}), I is the discharge current, t is the time of discharge, ΔV is the voltage difference between the upper and lower potential limits (0.9 V), and m is the mass of MnO_2 (0.4 mg cm^{-2}) which is estimated by Faraday law on the assumption that faraday current efficiency for deposition is 100%. As shown in Fig. 7b, the as-prepared MnO_2-based electrode delivers a SC of 385 F g^{-1} at a current density of 5 A g^{-1}, and the capacitance slowly decreases with the growth of current densities because there is no enough time for electrolyte ions to react with active materials in the quicker charge–discharge processes, which results in less active material being utilized and limited SC values. However, the capacitance retention ratio still reach circa 85% with growth of current densities from 5 to 15 A g^{-1}, indicating that high capacitance of the electrode can be obtained even at very high-power densities, which further confirms the superior rate capability of the electrode. Clearly, the high SC and excellent rate capability stem from the unique hierarchical porous structure of the electrode, in which electrolyte ions can easily transport to the surface of active material; as a result, the utilization efficiency is accordingly improved even at very quick charge/discharge processes.

The electrode was also subjected to a cycle life test at a current density of 5 A g^{-1}. Figure 8 shows the variation of specific capacitances with cycle numbers within a potential window of −0.05 ~ 0.85 V. It is observed that the SC of the electrode is 385 F g^{-1} during the initial stages of cycling, and there is hardly loss of capacitance as cycle increases with SC value of 374 F g^{-1} at the 2,000th cycle. It is obvious that the hierarchical porous MnO_2-based electrode also has a long-term electrochemical stability.

Conclusions

In summary, a hierarchical porous MnO_2-based electrode was prepared to maximize the utilization of MnO_2 for ECs. In this novel approach, porous MnO_2 was deposited onto a 3D porous gold-coated Ni foam by cathodic electrodeposition along with subsequent heat treatment at 200°C for 2 h. With the macropores of current collector as well as nanopores generated by dehydration during the heat treatment, the electrochemical performances of MnO_2 were greatly improved due to its high utilization efficiency. The electrode delivers a high specific capacitance of 385 F g^{-1} at a high current density of 5 A g^{-1} and exhibits excellent rate capability. The high specific capacitance and excellent rate capability of this hierarchical porous MnO_2-based electrode are advancements toward the ultimate goal of high energy and power densities for electrochemical capacitors.

Acknowledgments The authors acknowledge funding supports from the Major State Basic Research Development Program of China ("973" Program, No. 2009CB220100), the National High Technology Research and Development Program of China (863 Program, No. 2009AA033701), and Science and Technology Commission of Shanghai municipality (08DZ2270500), China.

References

1. Conway BE (1991) J Electrochem Soc 138:1539
2. Conway BE (1999) Electrochemical Supercapacitors-Scientific Fundamental and Technological Applications. Plenum, New York
3. Rudge A, Davey J, Raistrick I, Gottesfeld S (1994) J Power Sources 47:89
4. Ishikawa M, Morita M, Ihara M, Matsuda Y (1994) J Electrochem Soc 141:1730
5. Patel MN, Wang XQ, Wilson B, Ferrer DA, Dai S, Stevenson KJ, Johnston KP (2010) J Mater Chem 20:390
6. Zheng JP (2005) J Electrochem Soc 152:A1864

7. Kotz R, Carlen M (2000) Electrochim Acta 45:2483
8. Bian CQ, Yu AS, Wu HQ (2009) Electrochem Commun 11:266
9. Wu MS, Chiang PJ, Lee JT, Lin JC (2005) J Phys Chem B 109:23279
10. Chang JK, Hsu SH, Tsai WT, Sun IW (2008) J Power Sources 177:676
11. Toupin M, Brousse T, Bélanger D (2004) Chem Mater 16:3184
12. Pang SC, Anderson MA, Chapman TW (2000) J Electrochem Soc 147:44
13. Lee HY, Goodenough JB (1999) J Solid State Chem 144:220
14. Yuan CZ, Gao B, Su LH, Zhang XG (2008) J Colloid Interface Sci 322:545
15. Simon P, Gogotsi Y (2008) Nat Mater 7:845
16. Devaraj S, Munichandraiah N (2007) J Electrochem Soc 154:A901
17. Ghosh S, Inganas O (1999) Adv Mater 11:1214
18. Beguin F, Szostak K, Lota G, Frackowiak E (2005) Adv Mater 17:2380
19. Choi D, Blomgren GE, Kumta PN (2006) Adv Mater 18:1178
20. Cao L, Xu F, Liang YY, Li HL (2004) Adv Mater 16:1853
21. Prasad KR, Koga K, Miura N (2004) Chem Mater 16:1845
22. Soudan P, Gaudet J, Guay D, Belanger D, Schulz R (2002) Chem Mater 14:1210
23. Tian ZR, Tong W, Wang JY, Duan NG, Krishnan VV, Suib SL (1997) Science 276:926
24. Liu M, Zhang GJ, Shen ZR, Sun PC, Ding DT, Chen TH (2009) Solid State Sci 11:118
25. Kwon DK, Akiyoshi T, Lee H, Lanagan MT (2008) J Am Ceram Soc 91:906
26. Luo JY, Xia YY (2007) J Electrochem Soc 154:A987
27. Wang YG, Xia YY (2006) J Electrochem Soc 153:A450